Electrostatic ion-cyclotron waves in a nonuniform magnetic field

S. L. Cartier, N. D'Angelo, and R. L. Merlino
Department of Physics and Astronomy, The University of Iowa, Iowa City, Iowa 52242

(Received 22 April 1985; accepted 24 June 1985)

The properties of electrostatic ion-cyclotron waves excited in a single-ended cesium Q machine with a nonuniform magnetic field are described. The electrostatic ion-cyclotron waves are generated in the usual manner by drawing an electron current to a small exciter disk immersed in the plasma column. The parallel and perpendicular (to **B**) wavelengths and phase velocities are determined by mapping out two-dimensional wave phase contours. The wave frequency f depends on the location of the exciter disk in the nonuniform magnetic field, and propagating waves are only observed in the region where $f \gtrsim f_{ci}$, where f_{ci} is the local ion-cyclotron frequency. The parallel phase velocity is in the direction of the electron drift. From measurements of the plasma properties along the axis, it is inferred that the electron drift velocity is not uniform along the entire current channel. The evidence suggests that the waves begin being excited at that axial position where the critical drift velocity is first exceeded, consistent with a current-driven excitation mechanism.

I. INTRODUCTION

Electrostatic ion-cyclotron waves have been observed in laboratory plasmas[1] and in the auroral region of the magnetosphere,[2] while their presence in the solor corona[3] and in the Io plasma torus at Jupiter[4] has been suggested. This instability was first excited in a Q machine[5] by drawing a current to a small, positively biased disk, along the axis of a magnetized plasma column. Electrostatic waves with a frequency slightly in excess of the ion-cyclotron frequency were excited when the electron drift velocity exceeded about ten times the ion-thermal velocity and propagated radially outward from the current channel. The properties of these electrostatic ion-cyclotron waves were accounted for by Drummond and Rosenbluth,[6] for the case of an infinite, homogeneous, collisionless, magnetized plasma with a uniform electron drift along the **B** field. Since the initial experiments, ion-cyclotron waves have been the subject of numerous laboratory studies in which detailed comparisons with theory[7] were undertaken and measurements of ion heating associated with the instability[8] were also made.

Ion-cyclotron waves observed in the auroral region have also been associated with the presence of double layers,[9] and have been regarded as a possible acceleration mechanism for energetic (keV) H^+ and O^+ ions (so-called conics) that are observed, at times, to flow upward along the diverging magnetic field lines into the magnetotail.[10] The first theoretical study of ion-cyclotron waves appropriate to the auroral region was presented by Kindel and Kennel.[11] Theoretical and observational studies continue to investigate the excitation mechanism(s) for the auroral electrostatic ion-cyclotron waves.

Following the initial discovery[5] and theoretical[6] interpretation of ion-cyclotron waves, certain apparent discrepancies between Drummond and Rosenbluth's theory and new experiments were pointed out by Levine and Kuckes.[12] In particular, their experiments[12] showed that the critical drift velocity increased with increasing electron temperature, in contradiction to the predictions of the (collisionless) Drummond and Rosenbluth theory.[6] Levine and Kuckes[12] were thus led to seek an alternative excitation mechanism for the ion-cyclotron waves other than the current-driven mechanism. They suggested that the oscillations were destabilized by a negative resistance associated with the sheath in front of the positively biased exciter disk. However, the experiments were not performed under completely collisionless conditions, and when the current-driven theory was extended to include ion–ion collisions,[13] the predicted dependence of the critical drift on electron temperature was found to account for the experimental results of Levine and Kuckes.

For the reasons indicated above, the mechanism[12] based on a negative resistance associated with the disk sheath has been largely discounted. Recently Hatakeyama *et al.*,[14] based on their experiments in a nonuniform magnetic field, have suggested that the electrostatic ion-cyclotron instability is excited by a localized two-dimensional potential structure around the collecting disk. Their conclusion is based on the observations that (a) when the current-collecting disk was moved in regions of nonuniform magnetic field, or (b) when a local magnetic variation limited to the disk region was introduced, the electrostatic ion-cyclotron instability appeared along the entire current channel with a frequency approximately equal to the ion-cyclotron frequency determined by the (local) magnetic field strength at the position of the collecting disk. This two-dimensional sheath excitation mechanism was further investigated by Schrittwieser *et al.*[15] in a single-ended Q machine in which the usual disk collector was replaced by two concentric electrodes (a disk and a ring). In addition to the electron current drawn to the disk, large radial electric fields could be generated by biasing the disk relative to the ring. They found that the electrostatic ion-cyclotron instability was *not* excited when a strong two-dimensional sheath was present around the electrodes. The instability appeared only when the axial electron current exceeded the "conventional threshold," irrespective of the presence (or absence) of large radial potential gradients.

The effects of various nonuniformities (e.g., the finite width of the current channel) were already known since the first laboratory experiments on the electrostatic ion-cyclotron instability and, more recently, from, e.g., the work of Hatakeyama and Sato.[16] Some of these effects have recently

 0031-9171/85/103066-08$01.90

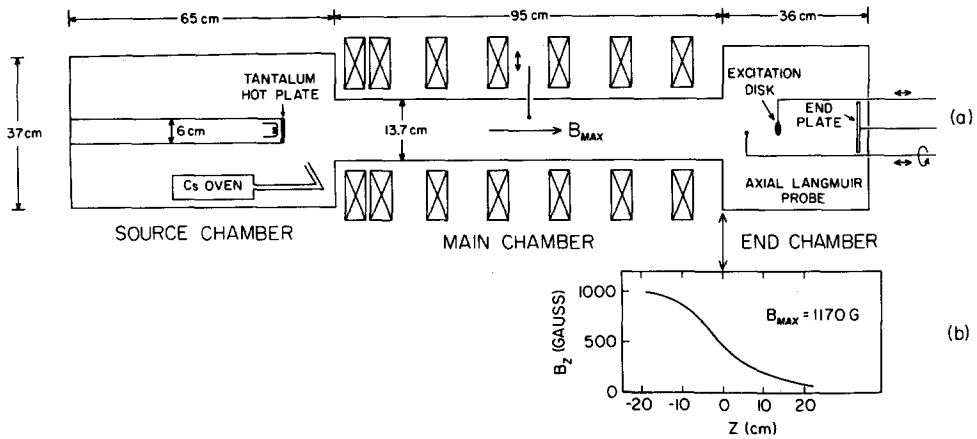

FIG. 1. Iowa Q machine. (a) Schematic cross-sectional view. (b) Axial variation of the B_z field in the region near and into the end chamber for a maximum field in the center of the main chamber of $B_{max} = 1170$ G. The arrows indicate the actual location of the $z = 0$ position in parts (a) and (b).

been considered in the nonlocal theories of, e.g., Ganguli and Bakshi,[17] and Bakshi, Ganguli, and Palmadesso.[18] They find that if the width of the current channel is reduced to a few ion Larmor radii the instability is completely quenched.[18] A systematic test of this "filamental quenching" phenomenon has been previously described.[19]

Here we report on our investigations of the excitation and propagation of ion-cyclotron waves in a nonuniform magnetic field. The experiments were performed in a single-ended Q machine that contains, in addition to the usual uniform magnetic field region, a region of nonuniform **B** field. The electrostatic ion-cyclotron wave frequency was measured for various positions of the current-collecting disk in the uniform and nonuniform field region. In this geometry measurements of the radial and axial propagation characteristics were made to determine parallel and perpendicular wavelengths and the direction of the wave phase velocity. The results show that the critical drift mechanism may still be applicable, and suggest an explanation for the dependence of the wave frequency on disk position.

A description of the apparatus and measurement techniques is given in Sec. II. The experimental results are presented in Sec. III, and the implications of these results are discussed and summarized in Sec. IV.

II. EXPERIMENTAL APPARATUS

The experiment was performed in a single-ended Q machine shown schematically in Fig. 1(a). The plasma is produced by surface ionization of cesium atoms sprayed onto a hot (~2200 °K) tantalum plate 6 cm in diameter (under electron-rich conditions) and is confined radially by an axial magnetic field variable up to 5 kG. The magnetic field is nonhomogeneous near the end of the device and its strength decreases rapidly with increasing z as one moves into the end chamber, where the plasma is terminated by a large, cold, electrically floating end plate as shown in Fig. 1(b). The ion-cyclotron instability is excited by biasing a movable metallic exciter disk at $V_D \approx 1$–2 V above the plasma potential to draw an electron current along the axis of the device. It is detected either in the electron-current oscillations of the disk itself or in the ion-current oscillations of various (axially and radially movable) disk Langmuir probes, 0.8 mm in diameter. Propagation measurements were made by triggering a dual-beam oscilloscope on the exciter disk current oscillations (at a fixed location) and observing the spatial change in phase seen on a movable probe. Typically the plasma density n is in the range $(10^9$–$10^{10})$ cm^{-3}, with plasma temperatures $T_e = T_i \cong 0.2$ eV. The chamber walls are cooled below 0 °C to keep the neutral cesium vapor pressure below 10^{-6} Torr.

III. EXPERIMENTAL RESULTS

As already stated in Sec. II, ion-cyclotron waves were excited by drawing current to a metallic disk, movable along the axis of the device and biased slightly above the plasma space potential. The instability was detected either in the current oscillations of the disk itself or by means of various (axially and radially movable) Langmuir probes. Figure 2 is a plot of the oscillation frequency, as detected by the (movable) exciter disk or by a probe fixed at $z = -47.5$ cm, for various positions of the exciter disk in the uniform and nonuniform magnetic field regions. The ion-cyclotron frequency at the exciter disk location is also shown for comparison. When the disk is located in the high (almost uniform) **B** region, the observed frequency is ~10% higher than the ion-cyclotron frequency, in general agreement with previous experiments[5] performed in uniform magnetic fields. However, when the

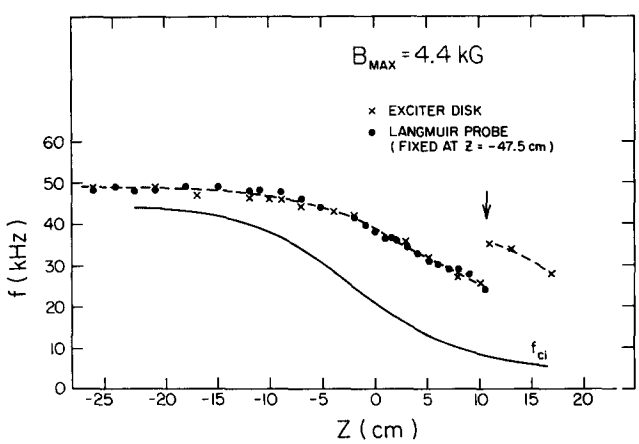

FIG. 2. Wave frequency versus exciter disk (0.64 cm radius) position (×). Oscillation frequency detected by a fixed Langmuir probe in the center of the main chamber, $z = -47.5$ cm (●). The arrow indicates the disk position at which excitation of the fundamental mode ceases. The solid line is the local ion-cyclotron frequency.

disk is located in the nonuniform field region, the observed frequency may be as large as 2–3 times the local ion-cyclotron frequency. Thus, in our case, it is no longer true that the waves are invariably excited with a frequency slightly above the local ion-cyclotron frequency at the location of the disk. We also note in Fig. 2 that the same frequency is observed in the disk current oscillations and on the fixed Langmuir probe located, within the current channel, in the high-**B** region.

As the exciter disk is moved to regions of lower **B** field, the ratio, $r_{ci}(z)/r_c(z) \propto 1/\sqrt{B}$, of the ion gyroradius to the radius of the current channel increases. Experimentally we found that when the width of the current channel becomes comparable to the local ion gyroradius near the position of the disk, excitation of the instability ceases. For the particular conditions of Fig. 2, the arrow indicates the location at which excitation of the fundamental mode ceases. This is an example of the *filamental quenching* accounted for in the nonlocal theory of Bakshi *et al.*[18] Further examples of this effect, for various disk diameters and magnetic field strengths, have been previously presented.[19]

The information given in Fig. 2 does not, by itself, allow us to determine whether excitation of the instability occurs near the disk (with a frequency f, however, that can be as large as 2–3 $f_{ci,\text{disk}}$) or somewhere well upstream of the disk, with $f \approx f_{ci,z^*}$, where z^* is some suitable upstream position. Further observations of the wave properties (to be reported next) appear, however, to be consistent with the latter hypothesis.

A. Wave propagation measurements

For a fixed exciter disk position, the propagation properties of the ion-cyclotron waves were determined by comparing the phase of the oscillations on a movable Langmuir probe with the phase of the disk current oscillations. The perpendicular and parallel wavelengths, as well as the direction of the parallel phase velocity, were determined by moving the Langmuir probe both radially and axially. As an example, results obtained from moving the probe radially at $z = 2.0$ cm, for a disk location of $z = -1.5$ cm, are given in Fig. 3. Evidently, the waves propagate radially outward from the current channel. Phase plots similar to Fig. 3, although not always of this quality, were made for different axial positions of the probe, so that constant phase contours could be constructed.

The equiphase contours are shown in Fig. 4, with several **B** field lines superimposed. The wave fronts are labeled by their respective phase angles, with wave propagation in the sense of increasing phase angle and a change by 360° equivalent to one wave period (for this case $T = 27$ μsec or $f = 37$ kHz). Ahead of the disk the waves propagate primarily radially although with a clear, finite component of the propagation vector along **B**. The earliest phases are observed upstream of the disk, indicating axial propagation toward the disk, i.e., in the direction of the electron drift. Behind the disk the waves tend to become acoustic-like. An especially significant feature in the data of Fig. 4 is the *absence* of wave propagation in the high-B region, namely at axial positions upstream of $z \approx -10$ cm. At the observed frequency of

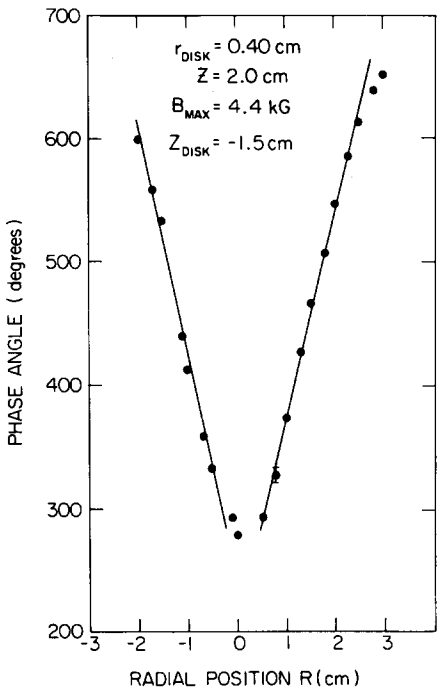

FIG. 3. Phase of the ion current oscillations on a Langmuir probe versus its radial position at $z = +2.0$ cm for a disk location of $z_D = -1.5$ cm.

$f = 37$ kHz, $f \cong f_{ci}$ at $z = -10$ cm, indicating that wave propagation is possible only in regions where $f > f_{ci}$. Oscillations within the current channel (but no propagating waves) are observed in the upstream region where $f < f_{ci}$, and the phase contour labeled 100 is extended upstream of $z \approx -10$ cm to indicate this.

Another interesting question is the variation, with axial position, of the perpendicular wavelength $\lambda_\perp$. In Fig. 5 the perpendicular wavelength $\lambda_\perp$, obtained from radial phase plots similar to those shown in Fig. 3 but with the disk located at $z = +12$ cm, is plotted versus z. For this particular case, the measured $\lambda_\perp$ (open circles) increases from ≈ 2 cm near the disk to ≈ 6 cm at $z \simeq -3$ cm. Beyond $z \simeq -3$ cm no wave propagation is observed. For comparison, the $\lambda_\perp$'s computed from the usual dispersion relation for electrostatic ion-cyclotron waves, i.e., $\omega^2 = \omega_{ci}^2 + k_\perp^2 C_s^2$, where ω is the measured wave frequency, ω_{ci} the ion-cyclotron frequency, C_s the ion-acoustic speed, and $k_\perp = 2\pi/\lambda_\perp$, are shown as the solid curve in Fig. 5. The appropriateness of using this dispersion relation in our nonhomogeneous magnetic field geometry is discussed in Appendix A, where it is shown that if the parallel wavenumber k_z and its spatial derivatives are negligible, then the uniform **B**-field dispersion relation remains approximately valid, with ω_{ci} and $k_\perp$, however, both being functions of z, i.e.,

$$\omega^2 \simeq \omega_{ci}^2(z) + C_s^2 k_\perp^2(z) . \tag{1}$$

Note that Eq. (1) predicts that the perpendicular wavelength is a real quantity only for axial positions at which $f > f_{ci}$, i.e., where, in the experiment, propagation outward from the current channel is observed.

The $\lambda_\perp$'s computed from Eq. (1), with $\omega = 2\pi f = 2\pi \times 27.4$ kHz, and with $\omega_{ci}(z)$ obtained from the measured values of the magnetic field strength, are in good agreement

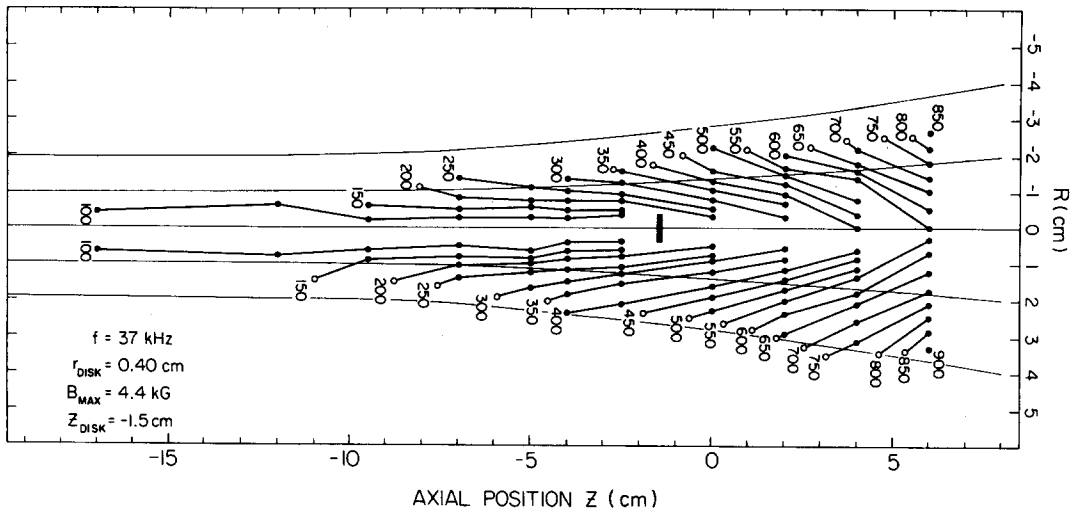

FIG. 4. Constant phase contours for a disk location $z_D = -1.5$ cm. The solid dots are data obtained from phase plots of the type illustrated in Fig. 3. The open circles are obtained by interpolation. Wave propagation is in the direction of increasing phase angle. A few B field lines are shown.

with the measured wavelengths. The value of $T_e = T_i = 0.2$ eV used in the computation is probably somewhat low and a better fit is obtained if slightly higher values are used. We have also considered the possibility that a Doppler-shift term should be added in the dispersion relation, since in our diverging magnetic field geometry we expect an (accelerated) plasma flow toward the low-B region, i.e., in the direction of the parallel phase velocity of the waves. Further discussion of the acceleration effect is given in Appendix B, but experimental evidence of the accelerated plasma flow is already present in the data of Fig. 4. On axis, behind the disk, the waves propagate essentially as ion-acoustic waves, so that $f\lambda_\parallel = v_{ph} = C_s + v_i$, v_i being the ion flow speed. Estimating $\lambda_\parallel$ to be ≈ 6 cm, and with $f = 37$ kHz, we find $v_{ph} = f\lambda_\parallel$ 2.2×10^5 cm/sec. With $C_s \approx 0.6\times10^5$ cm/sec, one finds that $v_i = v_{ph} - C_s \approx 1.6\times10^5$ cm/sec, giving a Mach number ($M \equiv v_i/C_s$) equal to 2.7, in agreement with estimates from Eq. (B4). If we take the flow speed to be $v \approx 10^5$ cm/sec *ahead* of the disk, then, as an upper limit to the Doppler shift there (where $\lambda_\parallel \gtrsim 20$ cm), we obtain $(\mathbf{k}\cdot\mathbf{v})/2\pi < 5$ kHz. The effect of this Doppler shift would mostly be to displace the computed $\lambda_\perp$ curve in Fig. 5 somewhat to the right.

Figure 6 shows an axial profile of the ion-cyclotron wave amplitude, $\delta n/n$, near the axis obtained by moving a small Langmuir probe along z, for a fixed disk position of $z_D = -1.5$ cm. The wave amplitude is small in the region where $f = f_{ci}(z)$ and increases monotonically toward the disk, typically reaching values of $\approx 30\%$.

The electrostatic ion-cyclotron wave amplitude and frequency also depend on the bias voltage of the disk. Figure 7(a) shows the variation of the observed wave frequency with $V_D - \phi_{PL}$, the disk bias, V_D, relative to the plasma space potential, ϕ_{PL}, for various fixed disk locations. In each case the observed frequency is above the local f_{ci} at the disk position, and generally increases with increasing bias. For the furthest upstream disk position (-12.2 cm), the frequency is independent of the bias. The wave amplitude at the disk is also shown in Fig. 7(b), for a disk located at $z = 2.3$ cm, as a function of $(V_D - \phi_{PL})$.

The question of how the wave frequency can depend on the exciter disk position and yet be consistent with a "critical

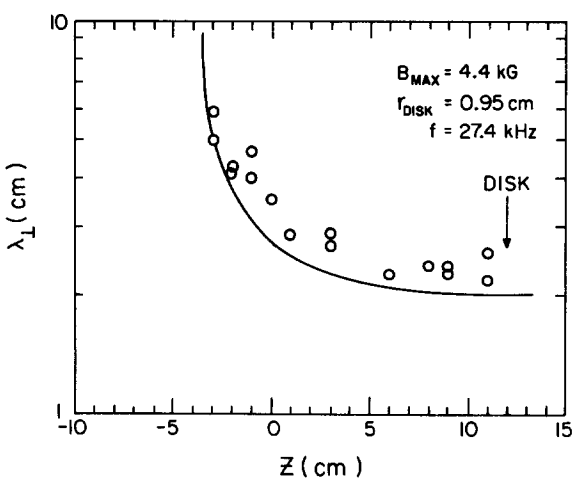

FIG. 5. Axial variation of the perpendicular wavelength for a disk located at $z_D = 12$ cm. The $\lambda_\perp$'s were obtained from phase plots, as in Fig. 3. The solid curve shows the $\lambda_\perp$'s obtained from Eq. (1) for the (constant) wave frequency $f = 27.4$ kHz and the measured B field values.

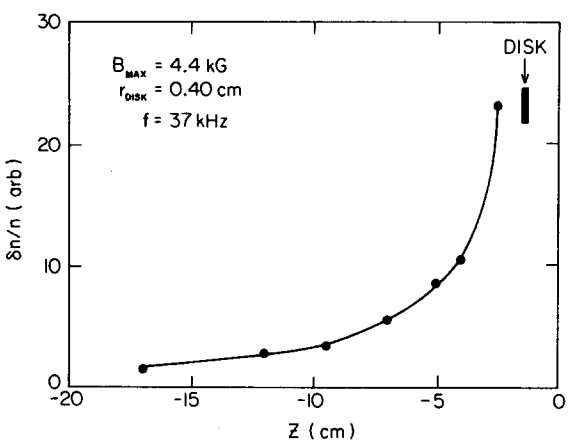

FIG. 6. Ion-cyclotron wave amplitude $\delta n/n$ versus z for a disk located at $z_D = -1.5$ cm. Typically $\delta n/n \approx 30\%$ near the exciter disk.

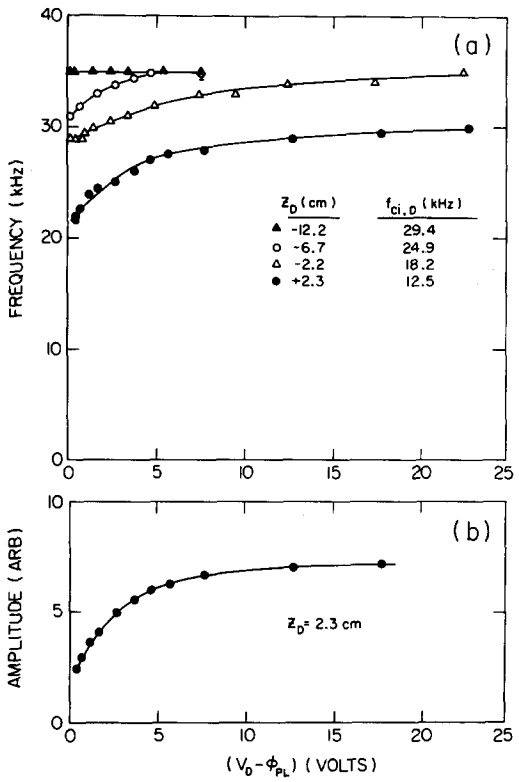

FIG. 7. The effect of disk bias. (a) Wave frequency versus disk bias (above the space potential) for various disk locations. (b) Wave amplitude at the disk versus disk bias for $z_D = +2.3$ cm. The disk radius was 0.95 cm.

drift" excitation mechanism will be addressed after some additional measurements pertaining to wave excitation are presented. Before proceeding we summarize the results on wave propagation as follows.

(1) Propagating ion-cyclotron waves are observed only in regions where the observed frequency is greater than f_{ci}. In these regions the waves propagate primarily radially outward from the current channel. The axial propagation is in the direction of the electron drift, with increasing amplitude along the drift.

(2) In regions where the magnetic field is nonuniform, the perpendicular wavelength changes to maintain a constant wave frequency as ω_{ci} varies, thus satisfying the approximate dispersion relation given in Eq. (1).

(3) For a disk located in the nonuniform **B** region, the wave frequency increases with increasing disk bias voltage and approaches the frequency observed when the disk is in the uniform **B** region.

B. Wave excitation

The wave propagation properties described under Sec. III A already suggest that, in order to clarify the wave excitation mechanism, we look in greater detail at the situation prevailing in a region extending some 15–20 cm upstream from the disk, rather than at a much more restricted region in the immediate vicinity of the disk, such as the sheath that must be present when the disk is biased at a few volts above the plasma potential. Perhaps the most cogent reason for doing so is the observation that, generally, the waves first appear some 15–20 cm ahead of the disk and that they exhibit a parallel phase velocity directed *toward* the disk, together with a wave amplitude that increases monotonically along the electron drift. To understand the general plasma conditions that may be conducive to wave excitation, we performed several sets of measurements of the space potential and of the plasma density upstream from the disk.

Figure 8 shows a series of radial scans of the floating potential measured by a Langmuir probe, the axial position of the probe being varied in steps between $z = -32$ cm and $z = 11.5$ cm. The disk location in this case was $z_{\text{disk}} = 12$ cm. For an electron temperature $T_e \simeq 0.2$ eV, scans of the floating potential are practically equivalent to scans of the plasma potential. With the disk bias $V_D = +2$ V of Fig. 8, a central current filament clearly appears from this type of measurements and is indicated in the figure by the dotted lines. In general, the radial **E** fields at the edges of the current channel are small, as can be inferred from any one of the radial potential scans in Fig. 8. The largest **E** fields must occur within a sheath of at most a few millimeters, just in front of the disk and well away from the axial position at which wave excitation first appears and the wave frequency equals the local gyrofrequency.

Information as to the plasma density in the region ahead of the disk was obtained also by means of a Langmuir probe. Figure 9 shows a series of radial scans of the ion-saturation current to a negatively biased probe (-6 V), the axial position of the probe being varied in steps between $z = -8$ cm and $z = +6$ cm. The disk location in this case was $z_{\text{disk}} = +8$ cm and the disk was biased at $V_D = +6$ V to collect electrons. A density depression near $R = 0$ cm is evident in Fig. 9 on each of the radial profiles and is more pronounced as one moves closer to the disk. The density depression is absent when the disk is left electrically floating.

The observation of a density depression when the disk is biased to collect electrons is not new. It has, in fact, been

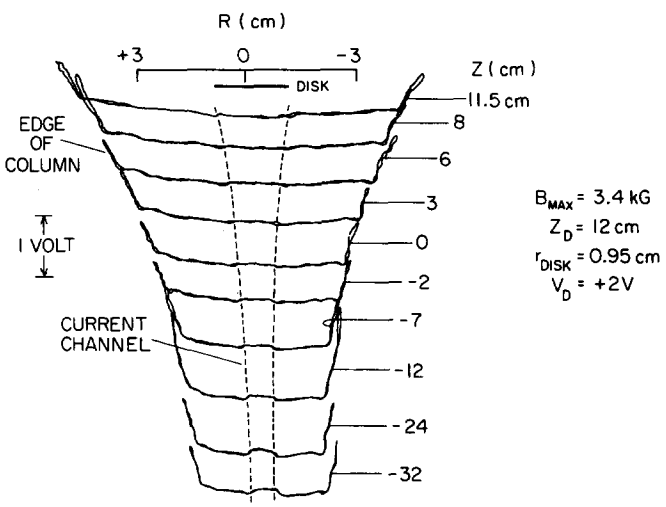

FIG. 8. Radial plots of the floating potential of a Langmuir probe for various axial positions between $z = 11.5$ cm to $z = -32$ cm. The dotted lines join the edges, in each plot, of the central current channel that is revealed by this type of measurement. For clarity each plot is displaced vertically (not to scale).

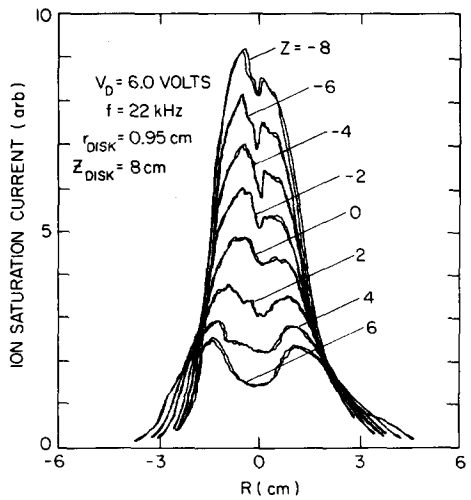

FIG. 9. Radial scans of the ion-saturation current to a negatively biased Langmuir probe at various axial positions. The density depressions appear near $R = 0$ when the exciter disk is biased to collect electron current.

reported by several authors[20,21] for a plasma immersed in a uniform magnetic field. What our present observations suggest, however, since the depression is more pronounced closer to the disk, is that a density *cavity* exists (presumably related to the removal of electrons to the disk), which extends from the disk into the high-B region. The density depression is present even for bias voltages of the disk somewhat below the critical voltage for wave excitation, but it rapidly increases in depth near the disk and affects the axial density profiles farther ahead of the disk as the bias voltage is increased. This behavior may be associated with the rapid increase in wave frequency with increasing bias voltage, as shown in Fig. 7.

We think that the observation of a density cavity, in our present nonuniform-B configuration, is important since it suggests that the electron drift velocity along the current channel is not constant. It would, instead, increase monotonically within the cavity as one moves closer and closer to the disk. In this situation the Drummond and Rosenbluth[6] condition for wave excitation, $v_{e,D} > v_{\rm crit}$, would first be fulfilled at a position approximately 15–20 cm ahead of the disk, and propagating waves would only be observed from that position onward toward the disk, with a parallel phase velocity directed toward the disk (see end of Sec. III A). That, indeed, $v_{e,D}$ increases monotonically as one moves along the current channel closer and closer to the disk, can be seen as follows.

Let $I_D = en(z)v_{e,D}\,A\,(z)$ be the total current collected by the disk, where $A\,(z)$ is the cross-sectional area of the current channel. We assume the total current along the channel to be the same at any z and equal to I_D, and also that $A\,(z)$ can be directly computed from the disk area and from the known **B** field configuration, i.e., $A\,(z) = A_{\rm disk}\ B_{\rm disk}/B\,(z)$. We estimate the density $n(z)$ from the measured profiles of the ion-saturation current $I_i(z)$ (e.g., Fig. 9) through

$$I_i(z) \propto n(z)v_i(z)A_p\ ,$$

where $v_i(z)$ is the ion flow speed and A_p is the area of the Langmuir probe. Also, $v_i(z) = C_s\,M\,(z)$, where C_s is the acoustic speed and $M\,(z)$ the Mach number of the flow. Here $M\,(z)$ can be determined from the measured axial profile of B, using the relation (B4) derived in Appendix B. It follows that the z variation of $v_{e,D}$ is expressed by

$$v_{e,D}(z) \propto I_D\ M\,(z)B\,(z)/I_i(z) \qquad (2)$$

in which all quantities of the rhs are measured quantities, except $M\,(z)$ which is computed as in Appendix B.

Normalized plots of the drift velocity computed from (2) are shown in Fig. 10 for several disk biases. As expected, $v_{e,D}$ increases monotonically toward the disk and, at any z, with increasing disk bias. As we argued above, wave excitation would first occur where $v_{e,D} = v_{\rm crit}$, and this position would then set the wave frequency. The arrows in Fig. 10 indicate the locations where, for each disk bias, the wave frequency f equals the local f_{ci}. All this is consistent with the observations summarized at the end of Sec. III A, in particular with points (1) and (3). With reference to point (3), note that, if wave excitation begins at the location where $f = f_{ci}$, then the increase in frequency from 19.5 to 24.5 kHz as V_D is increased from -1.4 to $+14.2$ V (Fig. 10) appears entirely reasonable on the basis of the measured axial variation of the drift velocity.

Unfortunately, we could not determine with great accuracy the absolute $v_{e,D}$'s in Fig. 10, primarily because of uncertainties in the determination of the absolute plasma density in the presence of a supersonic and axially variable flow. However, the estimated values of $v_{e,D}$ at the locations where $f = f_{ci}$ (see arrows in Fig. 10) were in the range $v_{e,D} \approx (10 - 30)v_{i,T}$, where $v_{i,T}$ is the ion-thermal speed. These $v_{e,D}$'s are of the same order as predicted by Drummond and Rosenbluth[6] for the critical drift in a uniform plasma immersed in a uniform magnetic field. We do not know whether a substantial change of the critical drift should be expected when the magnetic field is not homogeneous.

IV. DISCUSSION AND SUMMARY

The results presented in Sec. III indicate that, at least under the nonhomogeneous magnetic field conditions of our experiments, the electron drift velocity is *not* constant along the entire current channel but varies significantly, especially in the region near the exciter disk. This result, combined

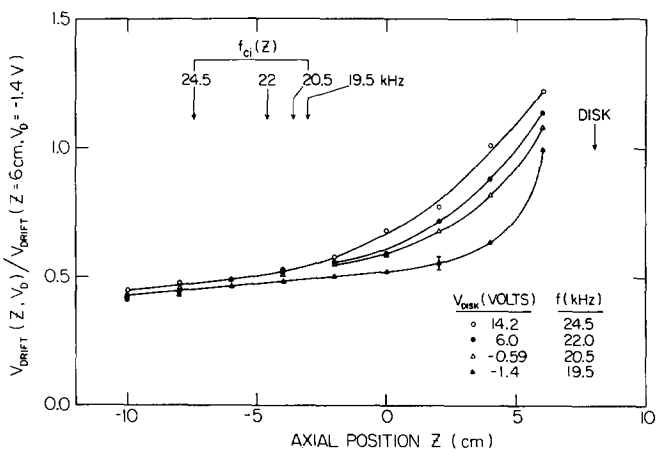

FIG. 10. Normalized axial plots (on axis) of the electron drift velocity for several disk bias voltages V_D. All plots are normalized to the $v_{\rm drift}$ value at $z = 6$ cm and $V_D = -1.4$ V. The arrows indicate the axial locations at which the observed wave frequencies f equal the local f_{ci}.

with the observed propagation characteristics, suggests that the ion-cyclotron waves are excited with a frequency which is determined at the axial position where the electron drift velocity first exceeds the critical value. The waves then propagate radially outward, with parallel propagation toward the disk in the direction of the electron drift. This latter feature is difficult to reconcile with the possibility that the waves are excited at the disk. Furthermore, the position where the wave frequency equals the local f_{ci} is, generally, well upstream of the disk, although the largest **E** fields appear within a few millimeters of the disk.

The position of initial wave excitation (where first $v_{e,D} > v_{\text{crit}}$) is determined by various plasma parameters and depends on the disk bias. In the presence of the current-collecting disk, an axial density cavity is formed with an extent that depends on the disk bias. For larger biases the cavity extends further into the high-**B** region and waves of higher frequency are excited. The wave frequency being apparently determined at the position of initial excitation, the waves continue to grow in amplitude as they propagate in the direction of the electron drift. This is seen not only in the axial profile of $\delta n/n$ (Fig. 6) but also in the dependence of wave amplitude on disk bias [Fig. 7(b)]. Figure 7(b), together with Fig. 10, suggests that at higher disk biases, excitation first occurs farther from the disk, so that wave growth may take place over a longer axial region.

It seems to us that our present results are well in line with the excitation mechanism originally proposed by Drummond and Rosenbluth[6] for a uniform plasma in a uniform magnetic field. Evidently, the nonuniformity of the magnetic field must introduce certain modifications such as, for instance, the axial variation of $k_\perp$ required for a constant ω when ω_{ci} varies axially [Eq. (1)]. In addition, the nonlocal effects discussed, e.g., by Bakshi *et al.*[18] have to be taken into account. They were experimentally demonstrated as the "filamental quenching" effect discussed at the beginning of Sec. III.

The present interpretation of our results is also in line with the recent work of Schrittwieser *et al.*,[15] who showed that even in the presence of a strong two-dimensional sheath around the exciter disk, the instability was only excited when the axial electron drift velocity exceeded a certain threshold.

It seems difficult at this stage, in spite of our present preference for the Drummond and Rosenbluth[6] excitation mechanism, to categorically exclude other mechanisms which have also been proposed (such as two-dimensional sheaths at the disk[16]), particularly in view of the fact that the latter mechanisms have not yet been analyzed to the same degree of thoroughness as the former.

One important point that has emerged from our observations is the axial nonuniformity of the electron drift, $v_{e,D}$; a possibility that had apparently not been given much attention previously. Perhaps some of the previous work on electrostatic ion-cyclotron waves should be partially reexamined in light of this new observation.

ACKNOWLEDGMENTS

We wish to thank Al Scheller for his expert technical assistance.

This work was supported by the United States Office of Naval Research and, in part, by NASA Grant No. NGL 16-001-043.

APPENDIX A: ELECTROSTATIC ION-CYCLOTRON (EIC) WAVE DISPERSION RELATION IN A NONHOMOGENEOUS B FIELD

We examine here briefly the question of why the dispersion relation for electrostatic ion-cyclotron waves in a uniform plasma in a uniform **B** field may continue to be approximately valid in our nonhomogeneous **B** configuration.

The linearized ion continuity and momentum equations read:

$$\frac{\partial \mathbf{v}_1}{\partial t} + n_0 \nabla \cdot \mathbf{v}_i = 0 , \tag{A1}$$

$$\frac{\partial \mathbf{v}_1}{\partial t} + C_s^2 \frac{1}{n_0} \nabla n_1 - \omega_{ci}(z) \mathbf{v}_1 \times \hat{z} = 0 , \tag{A2}$$

where n_0 is the zero-order plasma density, C_s is the ion-acoustic speed,

$$C_s = \{\kappa[(T_i + T_e)/m_i]\}^{1/2} ,$$

and n_1 and $\mathbf{v}_1$ are the first-order density and ion velocity, respectively. The **B** field is directed along the positive z axis and its strength depends on the z coordinate ($\hat{z}$ is the unit vector along $+z$). However, the components of **B** perpendicular to the z axis are neglected, an approximation valid near the axis of our plasma column. With $n_1(\mathbf{r},t) = n_1(\mathbf{r}) e^{-i\omega t}$, $\mathbf{v}_1(\mathbf{r},t) = \mathbf{v}_1(\mathbf{r}) e^{-i\omega t}$, and $\xi(\mathbf{r}) = 1/n_0\, n_1(\mathbf{r})$, we obtain:

$$-i\omega\xi + \nabla \cdot \mathbf{v}_1 = 0 , \tag{A3}$$

$$-i\omega \mathbf{v}_1 + C_s^2 \nabla \xi - \omega_{ci}(z) \mathbf{v}_1 \times \hat{z} = 0 . \tag{A4}$$

Taking the gradient of (A3) and using the vector relation

$$\nabla^2 \mathbf{A} = \nabla(\nabla \cdot \mathbf{A}) - \nabla \times \nabla \times \mathbf{A} ,$$

we obtain

$$\nabla \xi = -i(1/\omega)(\nabla^2 \mathbf{v}_1 + \nabla \times \nabla \times \mathbf{v}_1) \tag{A5}$$

and, inserting (A5) into (A4),

$$\omega^2 \mathbf{v}_1 + C_s^2 \nabla^2 \mathbf{v}_1 + C_s^2 \nabla \times \nabla \times \mathbf{v}_1 - i\omega\omega_{ci}(z) \mathbf{v}_1 \times \hat{z} = 0 . \tag{A6}$$

We look for solutions of the form

$$\mathbf{v}_1(\mathbf{r}) = \bar{\mathbf{v}}_1 \exp\{i[K_x(z)x + K_z(z)z]\} , \tag{A7}$$

with $\bar{\mathbf{v}}_1$ a constant vector, and the K_x and K_z components of the propagation vector functions of the z coordinate.

With the (A7) choice of $\mathbf{v}_1(\mathbf{r})$, the gradient operator becomes

$$\nabla \rightarrow \left[iK_x(z), 0, i\left(K_z(z) + z \frac{dK_z}{dz} \right) \right]$$

or, defining the vector

$$\tilde{K}(z) \equiv \left(K_x(z), 0, K_z(z) + z \frac{dK_z}{dz} \right) ,$$

we have

$$\nabla \rightarrow i\tilde{\mathbf{K}}(z) ,$$

and from (A6)

$$\omega^4 - (\omega_{ci}^2 + C_s^2 \tilde{K}^2)\omega^2 + C_s^2 \tilde{K}_z \omega_{ci}^2 = 0 . \tag{A8}$$

Equation (A8) can be written as

$$\omega^4 - (\omega_{ci}^2 + C_s^2 K^2)\omega^2 + C_s^2 \omega_{ci}^2 K_z^2 - C_s^2(\omega^2 - \omega_{ci}^2) \times \left[z^2 \left(\frac{dK_z}{dz} \right)^2 + z \frac{d}{dz}(K_z^2) \right] = 0 . \quad \text{(A9)}$$

If K_z and its spatial derivatives are negligible, (A9) becomes

$$\omega^2 \approx \omega_{ci}^2(z) + C_s^2 K^2(z) , \quad \text{(A10)}$$

namely, the same dispersion relation obtained in the case of a uniform **B**. Now, however, $K(z)$ adjusts itself to the variation of ω_{ci} with z, to keep ω a constant.

APPENDIX B: PLASMA FLOW IN A MAGNETIC LAVAL NOZZLE WITH ELECTRICAL CURRENT

We give here some simple arguments to show that, in our magnetic field configuration and in the presence of an electrical current drawn to a disk located near the end of the device, the relative electron-to-ion drift velocity, $v_e - v_i$, should increase continuously as one approaches the disk. The magnetic field configuration of our device is a "Laval nozzle" configuration, as discussed, e.g., in Andersen *et al.*,[22] except for the fact that a current is now drawn to the disk.

We can treat the steady-state operation of that portion of our plasma which is denoted as the current filament, by

$$A(z) n v_i = \text{const} , \quad \text{(B1a)}$$

$$A(z) n v_e = \text{const} , \quad \text{(B1b)}$$

$$n m_i v_i \frac{dv_i}{dz} + \kappa T_i \frac{dn}{dz} + en \frac{d\phi}{dz} = -\eta e^2 n^2 (v_i - v_e) , \quad \text{(B2a)}$$

$$\kappa T_e \frac{dn}{dz} - en \frac{d\phi}{dz} = \eta e^2 n^2 (v_i - v_e) . \quad \text{(B2b)}$$

Here $A(z)$ is the cross-sectional area of the current filament, which is a function of z, the axial distance along the device, n is the plasma density, ϕ is the electrostatic potential, T_i and T_e are the ion and electron temperatures, respectively, and η is the plasma resistivity. By defining the flow Mach number M as $M = v_i / C_s$, with

$$C_s = \{ \kappa [(T_i + T_e)/m_i] \}^{1/2} ,$$

we obtain from (B1) the following equations:

$$M \frac{dM}{dx} + \frac{1}{n} \frac{dn}{dx} = 0 , \quad \text{(B3)}$$

$$\frac{M^2 - 1}{M} \frac{dM}{dx} = \frac{1}{A} \frac{dA}{dx} . \quad \text{(B4)}$$

These two equations are precisely the same as obtained by Andersen *et al.*[22] for the case of zero electrical current along **B**. Using (B1a) and (B1b), we write the total current to the disk as

$$I = e(1 - I_e/I_i) A n v_i , \quad \text{(B5)}$$

where $I_{i,e} = enAv_{i,e}$. Also from (B2a) and (B2b), we have

$$E = -\frac{d\phi}{dz} = -\frac{\kappa T_e}{e} \frac{1}{n} \frac{dn}{dz} + \eta \frac{I}{A(z)} . \quad \text{(B6)}$$

There are two contributions to the axial electric field, one associated with the density gradient, the other with the passing of a current. In our experimental setup the second term is much smaller than the first.

As for the electron-to-ion relative drift, $v_e - v_i$, it can be written as

$$v_e - v_i = (I_e/I_i - 1) v_i = C_s (I_e/I_i - 1) M(z) . \quad \text{(B7)}$$

Thus, under the Laval nozzle conditions of $M(z)$ increasing monotonically as one approaches the disk, the largest $(v_e - v_i)$'s should occur near the disk.

[1] See, for example, H. Böhmer, S. Fornaca, N. Rynn, and M. Wickham, Phys. Fluids **21**, 2208 (1981); D. Dakin, T. Tajima, G. Benford, and N. Rynn, J. Plasma Phys. **15**, 175 (1976); R. Schrittwieser, Phys. Fluids **26**, 2250 (1983).

[2] P. M. Kintner, M. C. Kelley, and F. S. Mozer, Geophys. Res. Lett. **5**, 139 (1978); P. M. Kintner, M. C. Kelley, R. D. Sharp, A. G. Ghielmetti, M. Temerin, C. Cattell, P. F. Mizera, and J. F. Fennell, J. Geophys. Res. **84**, 7201 (1979).

[3] See, for example, S. Hinata, Astrophys. J. **235**, 258 (1980).

[4] D. A. Gurnett and C. K. Goertz, Geophys. Res. Lett. **10**, 587 (1983).

[5] N. D'Angelo and R. W. Motley, Phys. Fluids **5**, 633 (1962); R. W. Motley and N. D'Angelo, Phys. Fluids **6**, 296 (1963).

[6] W. E. Drummond and M. N. Rosenbluth, Phys. Fluids **5**, 1507 (1962).

[7] D. L. Correll, N. Rynn, and H. Böhmer, Phys. Fluids **18**, 1800 (1975).

[8] D. L. Correll, H. Böhmer, N. Rynn, and R. A. Stern, Phys. Fluids **20**, 822 (1977).

[9] F. S. Mozer, C. W. Carlson, M. K. Hudson, R. B. Torbert, B. Parady, and J. Yatteau, Phys. Rev. Lett. **38**, 292 (1977).

[10] R. D. Sharp, R. G. Johnson, and E. G. Shelley, J. Geophys. Res. **82**, 3324 (1977).

[11] J. M. Kindel and C. F. Kennel, J. Geophys. Res. **76**, 3055 (1971).

[12] A. M. Levine and A. F. Kuckes, Phys. Fluids **9**, 2263 (1966).

[13] R. K. Varma and D. Bhadra, Phys. Fluids **7**, 1082 (1964).

[14] R. Hatakeyama, N. Sato, H. Sugai, and Y. Hatta, Phys. Lett. A **63**, 28 (1977).

[15] R. Schrittwieser, N. Rynn, R. Koslover, and R. Karim, Plasma Phys. Control. Fusion **26**, 1591 (1984).

[16] R. Hatakeyama and N. Sato, *Proceedings of the Plasma Conference* (Institute of Electrical Engineers, Tokyo, Japan, 1981), p. 31; N. Sato and R. Hatakeyama, J. Phys. Soc. Jpn. **54**, 1661 (1985).

[17] G. Ganguli and P. Bakshi, Phys. Fluids **25**, 1830 (1982).

[18] P. Bakshi, G. Ganguli, and P. Palmadesso, Phys. Fluids **26**, 1808 (1983).

[19] R. Schrittwieser, Phys. Fluids **26**, 2250 (1983); S. L. Cartier, N. D'Angelo, P. H. Krumm, and R. L. Merlino, *ibid.* **28**, 432 (1985).

[20] H. Böhmer and S. Fornaca, J. Geophys. Res. **84**, 5234 (1979).

[21] M. J. Alport, P. J. Barrett, and M. A. Behrens, Plasma Phys. Control. Fusion **25**, 1059 (1983).

[22] S. A. Andersen, V. O. Jensen, P. Nielsen, and N. D'Angelo, Phys. Fluids **12**, 557 (1969).